Path-length measurement performance evaluation of polarizing laser interferometer prototype

**Yu-qiong Li · Zi-ren Luo · He-shan Liu · Yu-hui Dong ·
Gang Jin**

Abstract The space laser interferometer has been considered the most promising means for detecting gravitational waves and improving the accuracy and spatial resolution of the Earth's gravity model. An on-ground polarizing laser interferometer prototype equipped with one reference interferometer and two measurement interferometers having equal-length arms is presented in the paper. The laser interferometer prototype is designed as the demonstration of a Chinese space laser interferometer antenna in the future, of which the path-length measurement performance evaluation and preliminary noise analysis are investigated here. The results show that the path-length measurement sensitivity is better than 200 pm/Hz$^{1/2}$ in the frequency band of 10 mHz–1 Hz, and the sensitivity of measuring the motion of a sinusoidally driven testmass is better than 100 pm within the frequency regime of 1 mHz–1 Hz. In this way, laboratory activities have demonstrated the feasibility of this prototype to measure tiny path-length fluctuations of the simulated testmass. As a next step, adopting an integrated design of optics and optical substrate to enhance the stability of the laser interferometer is being planned, and other key techniques included in the space laser interferometer such as laser pointing modulation and laser phase-locking control are to be implanted into this prototype are under consideration.

Yu-qiong Li and Zi-ren Luo Contributed equally to this work.

Y. Li · Z. Luo · H. Liu · Y. Dong · G. Jin (✉)
National Microgravity Laboratory (NML),
Institute of Mechanics, Chinese Academy of Sciences,
Beijing 100190, People's Republic of China
e-mail: gajin@imech.ac.cn

H. Liu · Y. Dong
University of Chinese Academy of Sciences, Beijing 100190,
People's Republic of China

1 Introduction

The space laser interferometer has been considered the most promising means for detecting gravitational waves with a possibility of opening a new astronomy window in the future. The laser interferometer space antenna (LISA) mission and LISA-like missions such as evolved laser interferometer space antennae (eLISA)/next gravitational observer (NGO) have been investigated for many years, and many key techniques including laser interferometer, microthruster and inertial sensor have been made great progress [1–13]. LISA consists of three spacecraft forming a triangle with 5 million km arm length, of which the spacecraft will move up to 15 m/s relative to each other due to the orbital mechanics [14]. The eLISA/NGO is just an abridged version of the LISA, which has only two measuring arms [15].

The gravity recovery and climate experiment (GRACE) has successfully demonstrated the use of K-band microwave inter-satellite ranging between two satellites in low-Earth orbit for monitoring the spatial and time variability of Earth's gravity fields, of which the Geoid accuracy and the spatial resolution are 1 cm and 350 km, respectively [16, 17]. The information gained about the global gravity fields from GRACE raised an interest in developing a follow-on mission with better performance to improve our knowledge of, for example, the cryosphere and hydrological or atmospheric phenomena affecting the Earth's system. This follow-on mission will be launched in 2017 [16, 18–21]. Besides the microwave inter-satellite ranging metrology system, the GRACE follow-on mission will carry a satellite-to-satellite laser interferometer for demonstrating the feasibility of long baseline space laser interferometer and improving the distance measurement precision between two satellites [22–25].

The advanced laser interferometer antenna (ALIA) mission was first proposed by Bender et al. [12, 13], and a feasibility study, carried out by a Chinese research group [26], promises to provide significant insights into the physics of intermediate mass black holes (IMBHs) [27–33]. The space advanced gravity measurement (SAGM) mission is designed for the Earth's gravity recovery proposed by China, of which the recommended inter-satellite distance is about 100 km and the precision of inter-satellite range monitoring is required to be better than 10 nm/Hz$^{1/2}$ at 0.1 Hz [26, 34, 35].

Between the above missions, many technical parameters such as satellite-to-satellite distance, measurement precision, measurement frequency band, and Doppler velocity are greatly different, but the technical requirement to measure the tiny differential position of two spacecraft is similar. Many issues including high measurement precision and wide frequency band make the laser interferometer become a challenging enterprise, but the Max Planck Institute for Gravitational Physics in Germany has made great progress, allowing the use of laser interferometer for satellite–satellite tracking become possible [1–3, 9, 14, 19, 21]. On November 28, 2013, European Space Agency (ESA) announced that the search for elusive gravitational waves called 'The Gravitational Universe' was selected as the third L-class mission, and becomes the most promising alternative [36–38]. In 2011, National Aeronautics and Space Administration (NASA) quit from the LISA mission, and ESA was seeking cooperation with China all this time. In China, an on-ground laser interferometer methodology demonstration has been built in our previous work [34], and here an upgraded laser interferometer prototype is presented, which is placed in a vacuum chamber and built on an optical bench for vibration isolation. The prototype depicted here is just a ground-based demonstrator for the SAGM and ALIA in China, the optical design of which is similar to that of LISA Pathfinder except for the adoption of polarizing light [39, 40]. The results show that the path-length measurement sensitivity of the prototype is better than 200 pm/Hz$^{1/2}$ in the frequency band of 10 mHz–1 Hz, and the performance of characterizing the motion of the simulated testmass is better than 100 pm within the frequency range of 1 mHz–1 Hz.

2 Design and experimental details

Considering the Doppler shift of LISA and GRACE follow-on missions, the heterodyne interferometer becomes an optimal path-length fluctuations readout scheme. Limited by the bandwidth of the photodiodes (4 kHz–5 MHz) and the modulation frequency range of the acousto–optic modulators (AOMs), modulation frequency range: 10 kHz–2 MHz, resolution: 1 kHz, the beat frequency of the interferometer system adopted is from 100 kHz to

2 MHz. The previous investigations showed that the system measurement error was almost the same, while the beat frequency varied from 100 kHz to 2 MHz. Thus, a 1-MHz beat frequency is adopted for simplifying the discussion in the paper.

2.1 Description of the experimental setup

To minimize the effects of thermal noise, electromagnetic noise and vibration noise on the ranging accuracy of the laser interferometer, an optical table with passive vibration isolation based on an isolated ground was adopted, on which a vacuum chamber was constructed. The schematic diagram of the experimental setup and the physical picture of the laser interferometer prototype are shown in Figs. 1 and 2, respectively. The vibration isolation system consists of an isolated ground and a suspended optical table, the resonance frequency of which is about 1 Hz. During the pumping process of the vacuum chamber, three pumps were used: a rotary pump, a turbo pump and an ion pump. However, the rotary pump and turbo pump would cause vibration noise, while the ion pump would bring thermal noise and electromagnetic noise. Thus, all the three pumps were all stopped after the pressure of the vacuum chamber reached 2×10^{-6} mbar, and thus the pressure may rise to about 10^{-3} mbar when the path-length fluctuations are being measured, which could take about 72 h.

As a polarizing layout is convenient to separate ingoing and returning beams [19, 41], here the proposed optical design adopts such a polarizing layout. The laser interferometer layout consists of a modulation bench and an optical bench, the schematic diagram of which is shown in Fig. 3. The modulation bench located outside of the vacuum chamber provides laser beam preparation. The linearly polarized light emitted from the laser (made in Beijing, wavelength $\lambda = 1{,}064$ nm, power $P = 300$ mW, frequency instability $\Delta f = 1$ MHz/2 h) passes through a Faraday isolator to avoid back-reflection of the laser beam. Then, the laser frequency is modulated by using AOMs at approximately 70 MHz with a frequency difference f_{het} of 1 MHz, the relative frequency instability of which is 10^{-7}. Finally, the frequency-shifted beams are injected into the optical bench in the vacuum chamber by two single-mode optical fibers. The role of the wedged plate is to make the laser beam emitted from the AOM's first diffraction become parallel to the optical bench.

The optical bench located in the vacuum chamber contains three interferometers with equal arm-length, performing the path-length fluctuations measurement, the physical picture of which is shown in Fig. 4. The reference interferometer senses the common-mode phase fluctuations caused by the environmental noises, such as mechanical

Fig. 1 Schematic diagram of the experimental setup
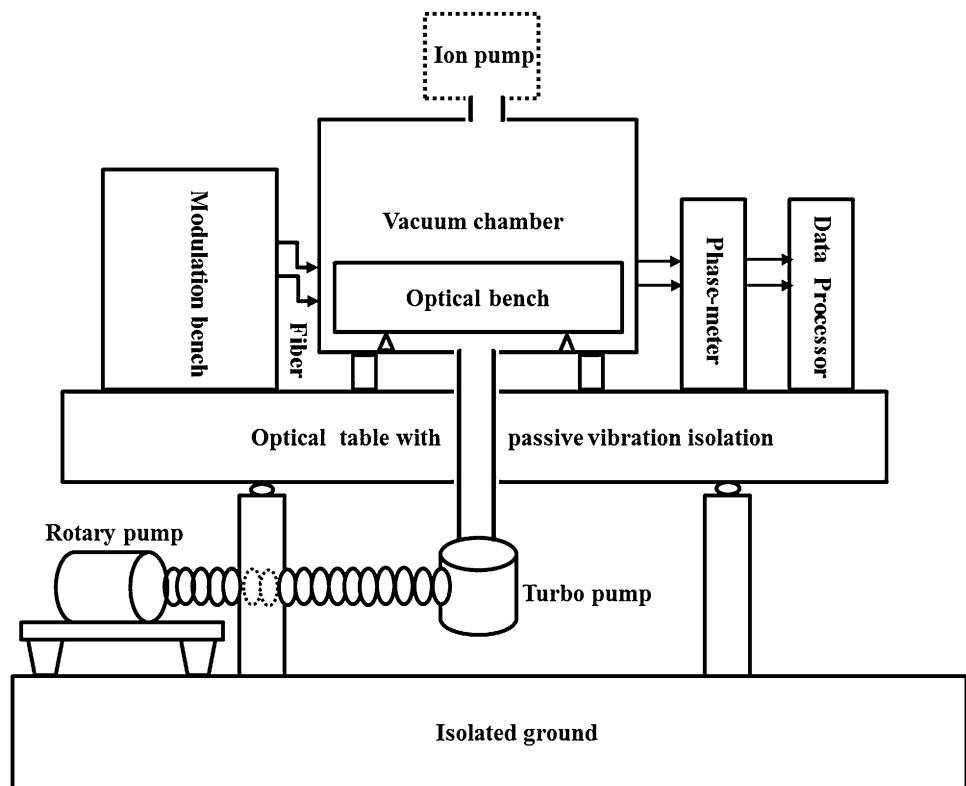
**Fig. 2** Physical picture of the laser interferometer prototype

and thermal fluctuations, which occur outside the stable optical bench, as shown in Fig. 5a. The testmass-bench measurement interferometer (TBMI) measures the relative path-length fluctuations between the simulated testmass (here replaced by a mirror installed on a nano-positioning stage) located on the left side of the optical bench and the optical bench, as shown in Fig. 5b. The testmass–testmass measurement interferometer (TTMI) is sensitive to the relative distance of the two simulated testmasses to each other, as shown in Fig. 5c. Path-length fluctuations of the modulation bench resulting from the environmental noises are measured in each individual interferometer and canceled in the differential phase 'R–M' ('R' and 'M' refer to the reference interferometer and the measurement interferometer, respectively). So, path-length differences before the optical bench are canceled by referring all measurements to the reference interferometer, and only those on the optical bench are coupled into the path-length ranging. The interferometer prototype was simulated by a software named Ifocad, which was invented by the Max Planck Institute for Gravitational Physics. The simulation results showed that the optical path difference and angular deviation between two interfering beams of each interferometer are only about 2 mm and 1.7×10^{-8} rad, respectively. However, only 1 mm of positioning accuracy and 1×10^{-4} rad of angle measurement accuracy for the components orientation were reached during the optical bench building, which were limited by the accuracy of the measurement method (a millimeter ruler was used as the measuring tool) utilized in the experiment. So, the total optical path-length difference ΔL and angular deviation $\delta\theta$ between the two interfering beams of the three laser interferometers were evaluated to be about 5 mm and 3×10^{-4} rad, respectively.
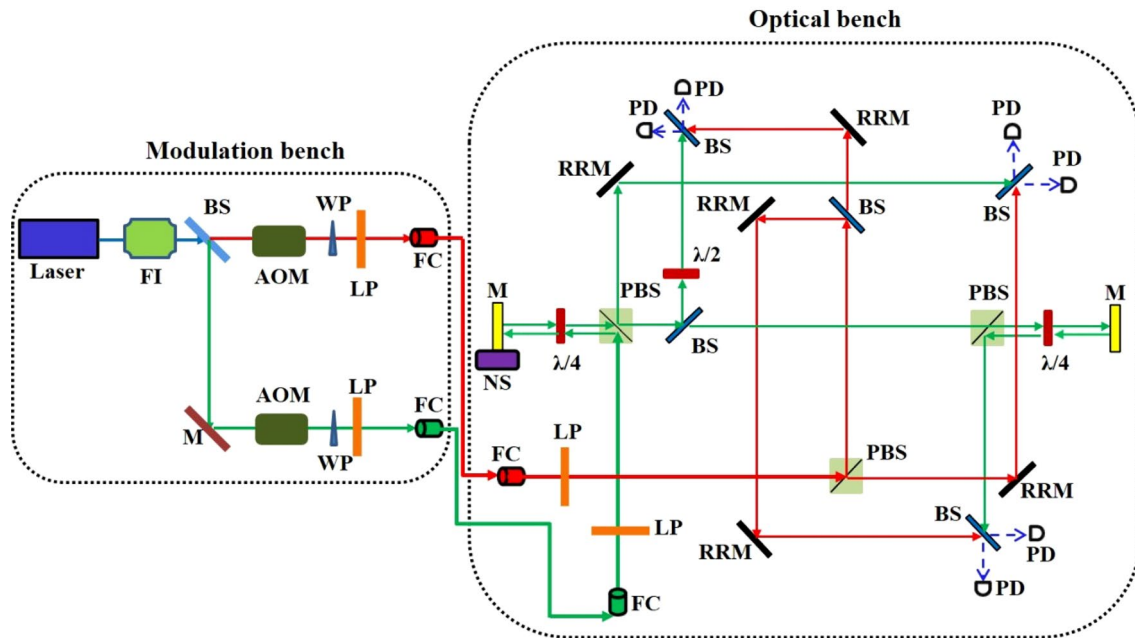
Fig. 3 Schematic diagram of the heterodyne interferometer. *FI* Faraday isolator, *BS* 50/50 beam splitter, *M* mirror, *AOM* acousto-optic modulator, *WL* wedged plate, *LP* linear polarizer, *FC* fiber coupler, *RRM* rectangular reflection mirror, *PBS* polarizing beam splitter, *PD* photo-detector, *NS* nano-positioning stage
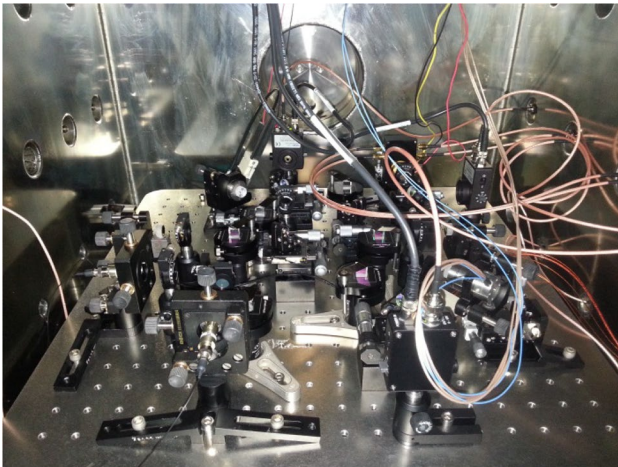
Fig. 4 Physical picture of the optical bench

2.2 Phasemeter

The relation between the relative path-length fluctuation and the interference signal's phase change is the following:

$$\delta L = \frac{\Delta\theta}{2\pi} \cdot \lambda$$

where δL is the path-length fluctuation, $\Delta\theta$ is the interference signal's phase change, λ is the laser wavelength. So, the readout scheme of relative path-length fluctuation δL

needs a phasemeter to detect the phase information of the interference signal.

The schematic diagram of a 'common noise rejection' phasemeter adopted in the experiment is shown in Fig. 6, the methodology of which is based on the digital phase locked loop (DPLL) [39]. The architecture is mainly based on a commercial field programmable gate array (FPGA) platform (Terasic, DE3-340). To avoid the effects of the laser frequency instability jitter noise and electronic device noise of the laser interferometer on the measurement accuracy evaluation of the phasemeter, a detected signal produced from an external function generator (Agilent, 33522A) was used. To simulate the interference signal of the prototype, the parameters of the detected signal are the following: peak to peak amplitude $A = 150$ mV, direct-current offset $B = 10$ mV, frequency $f = 1$ MHz. The phase noise of the phasemeter is shown in Fig. 7, from which can be seen that the phase noise is lower than 2×10^{-5} rad/Hz$^{1/2}$ in the higher frequency band from 10 mHz to 1 Hz, but the phase noise increases with decreasing frequency within the lower frequency regime of 0.1–10 mHz because of thermal effects [39].

3 Results and discussion

In order to shield the environmental disturbances as much as possible, all performance measurements were taken
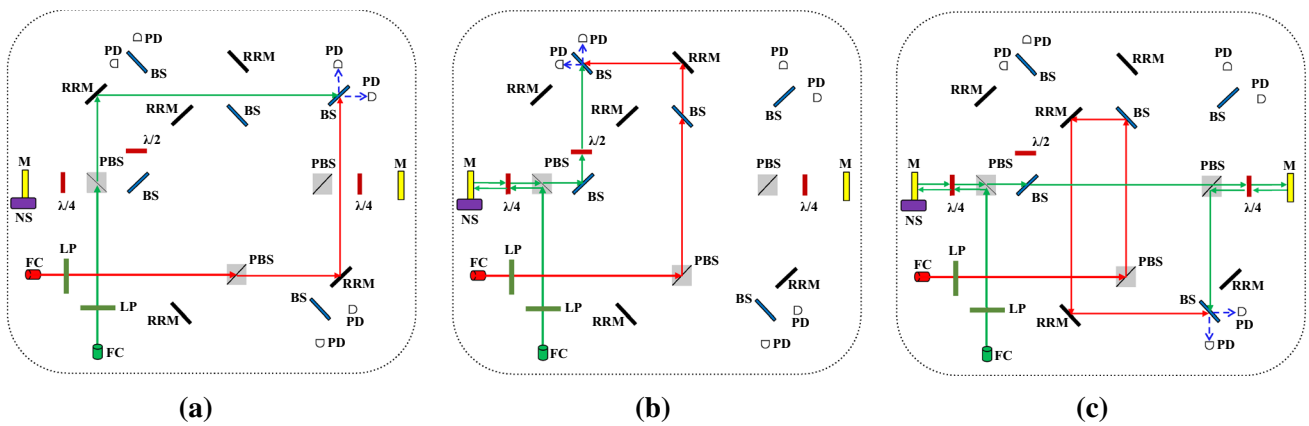
Fig. 5 Schematic diagram of the three interferometers. **a** the reference interferometer **b** the testmass-bench measurement interferometer **c** the testmass–testmass measurement interferometer
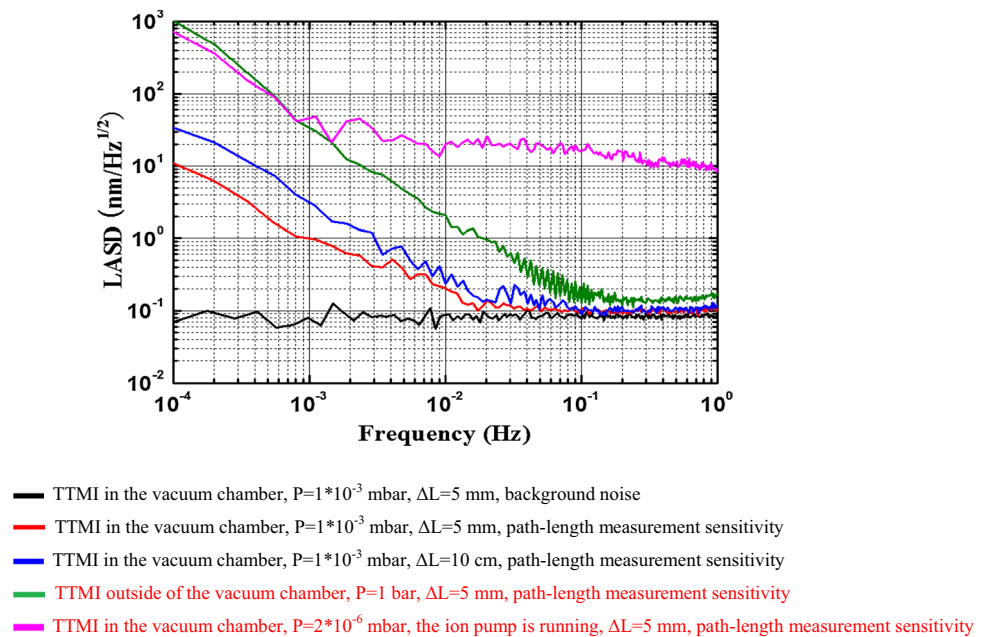
Fig. 6 Schematic diagram of the phasemeter
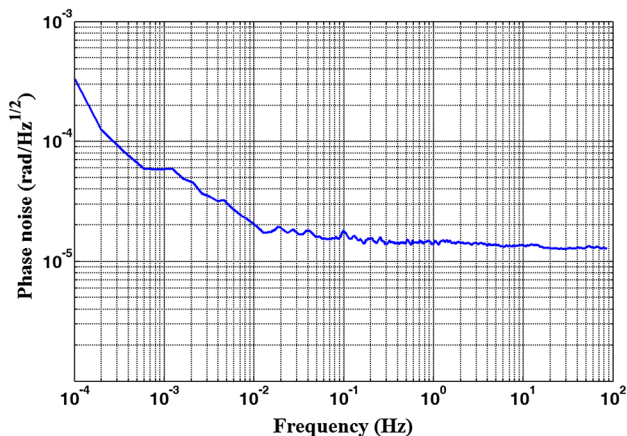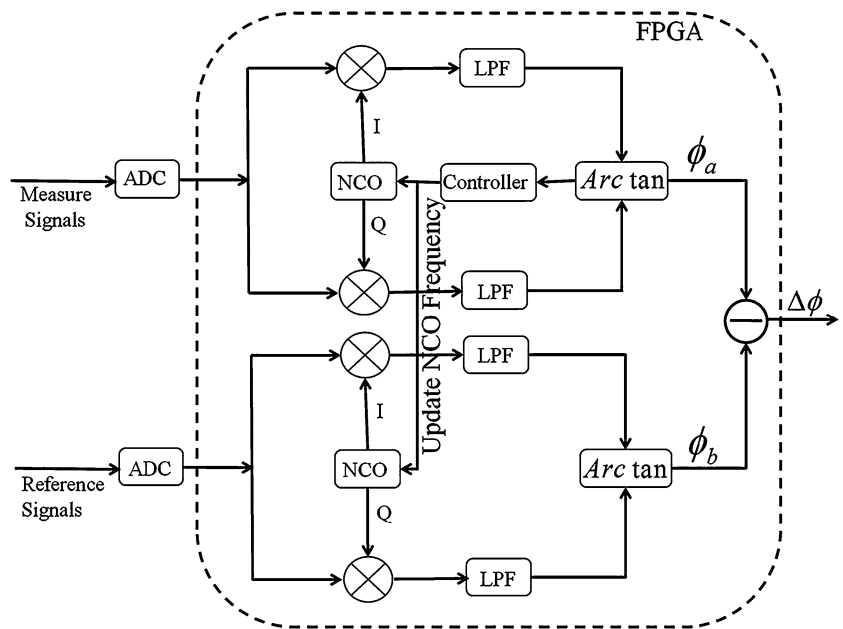
Fig. 7 Phase measurement noise of the phasemeter

over night. Out of several data stretches, the stretch of 1,000–10,000 s length was selected for the testing graphs that showed little external disturbances. The data were analyzed with a method called linearization amplitude spectral density (LASD), of which the toolbox was developed by the Max Planck Institute for Gravitational Physics. Many experiments have demonstrated that the TTMI has the same performance as the TBMI, so here only the TTMI is taken to be discussed for evaluating the measurement precision of the laser interferometer.

Before evaluating the path-length fluctuations sensitivity of the prototype, it is necessary to measure the background noise level of the laser interferometer prototype and phasemeter. The experimental setup is the following: dividing the TTMI's readout from one photodiode into two parts and

Fig. 8 Path-length measure-
ment sensitivity of the TTMI

TTMI in the vacuum chamber, P=1*10⁻³ mbar, ΔL=5 mm, background noise

TTMI in the vacuum chamber, P=1*10⁻³ mbar, ΔL=5 mm, path-length measurement sensitivity

TTMI in the vacuum chamber, P=1*10⁻³ mbar, ΔL=10 cm, path-length measurement sensitivity

TTMI outside of the vacuum chamber, P=1 bar, ΔL=5 mm, path-length measurement sensitivity

TTMI in the vacuum chamber, P=2*10⁻⁶ mbar, the ion pump is running, ΔL=5 mm, path-length measurement sensitivity

then adopting the phasemeter to measure the phase differ-ence between them. The black curve in Fig. 8 shows that the background noise of the prototype is about 100 pm/Hz$^{1/2}$ inside the frequency regime of 0.1 mHz–1 Hz. Compared with Fig. 7, the main noise is probably due to the low sig-nal-to-noise Ratio (SNR) of the interference signal.

3.1 Impact of vacuum chamber's shield on measurement sensitivity

To verify the impact of the vacuum chamber's shield on the path-length measurement sensitivity, the path-length meas-urement sensitivities of the TTMI placed in and outside of the vacuum chamber at room temperature are measured, which are shown as the red curve and the green curve in Fig. 8, respectively. When the chamber is evacuated, the noise contributions from air flow, acoustics, magnetic and electric fields, etc. are reduced, and the optical path length has much less noise from fluctuations of the air density in the beam's path. More important, the vacuum chamber's thermal shield provides a better thermal stability environ-ment for the laser interferometer. From the comparisons of the red curve and the green curve in Fig. 8, it can be seen that an improvement of two orders of magnitude has been achieved by the vacuum chamber's shield.

Comparing with the sensitivity distribution of the red and green curves at the lower frequencies in Fig. 8, it can be deduced that the main factor affects the ranging accuracy is the thermal noise resulting from the temperature fluc-tuation of the surrounding environment. It is because that there is only one air conditioner to adjust the room temper-ature, and it is the only thermostat. Besides, although the

vacuum chamber and invar steel optical bench are adopted, the mounting brackets of all components are made of alu-minum, the thermal expansion coefficient of which is only about 10^{-5}/°C, it is the weak point in the current design of the setup. So, the path-length measurement sensitivity of the TTMI in the vacuum chamber is better than 200 pm/Hz$^{1/2}$ in the frequency range of 10 mHz–1 Hz, but decreas-ing with a linear function with decreasing frequency within the frequency range of 0.1 mHz–0.1 Hz.

3.2 Impact of laser frequency instability on measurement sensitivity

In a heterodyne interferometer, the optical path-length dif-ference ΔL between two interfering beams and the laser fre-quency instability δf will be translated into phase fluctuation $\delta\phi$ at the heterodyne frequency, the relation of which is given by

$$\delta\phi = \frac{\Delta L}{C} 2\pi \delta f,$$

where c is the speed of laser light [41, 43]. According to the specification of the laser, it is known that the laser fre-quency instability $\delta f = 1$ MHz/2 h.

To investigate the impact of laser frequency instability on the path-length measurement sensitivity, an intentional arm-length difference of $\Delta L = 10$ cm was made based on the equal arm-length of TTMI (the original optical path-length difference ΔL is evaluated to be 5 mm) placed in the vacuum chamber. The blue curve in Fig. 8 demonstrates that the path-length measurement sensitivity has declined a half order of magnitude compared to that of the equal arm-length interferometer.

3.3 Impact of ion pump on measurement sensitivity

The ion pump adopted in this experiment is manufactured by the Agilent Technologies (VIP300), the ultimate pressure of which is about 10^{-11} mbar. But the minimum pressure of the vacuum chamber is about 2×10^{-6} mbar, which is limited by the leakage rate of the chamber (SUS 304) and the outgassing rate of the components utilized in the optical bench. The operating voltage between the cathode and anode plates of the ion pump is approximately 7,000 V, and the current between the two electrode plates is about 10 mA according to the instructions of the ion pump ($P = 2 \times 10^{-6}$ mbar). So, the heating power of the ion pump is about 70 W, which is a huge heat source for the laser interferometer. Besides, the strenuous exercise of the residual molecules and the large alternating current bring pulse perturbations to the measurement system, which probably results from the momentum transfer of statistically impinging molecules on the mirrors and the fluctuations in refractive index due to the statistical fluctuations of the number of molecules in the beam's path. All of these seriously affect the ranging accuracy of the laser interferometer, the measurement sensitivity of which while the ion pump is running is shown as the magenta curve in Fig. 8. Compared with the situation that the ion pump is shut off, it is indicated that the path-length measurement noise level becomes worse greatly. Therefore, how to further decrease the background pressure of the vacuum chamber to reduce the impact of the ion pump on the measurement sensitivity is an urgent task in the next step. And it also tells us that if we intend to make the ion pump work normally that doesn't bring pulse perturbations, the background pressure of the vacuum chamber should be lower than 10^{-8} mbar.

3.4 Impact of ultra-stable oscillator (USO) on measurement sensitivity

The relative frequency instability of the USO adopted by the AOMs in the experiment is about 10^{-7}, of which the central frequency is 70 MHz, so the frequency instability of the interference signal is approximately 7 Hz. The relational expression between the phase noise and the frequency instability of the detected signal has been obtained in the previous work, from which can be obtained that the absolute value of the USO jitter noise is no more than 1 pm [42]. Besides, for the USO adopted by the numerically controlled oscillator (NCO) of the phasemeter being unable to perfectly track the frequency of the tested signal, the phase noise of the USO results in sampling time errors that lead to frequency-dependent phase errors that are proportional to the beat frequency [21, 42].

3.5 Impact of laser pointing jitter on measurement sensitivity

In this experiment, the laser pointing jitter noise results from the instability of the optical components installed on the optical bench. A pointing jitter measurement method based on the differential wave-front sensing (DWS) technique is used to measure the laser beam pointing jitter, and the results show that the laser jitter noise is no more than 4 nrad/Hz^½ in the frequency band of 1 mHz–1 Hz. From the relation between the laser beam pointing jitter and the phase measurement error [21], it can be concluded that the maximum path-length fluctuation resulting from the laser pointing jitter is about 3.2 pm/Hz^½.

3.6 Analysis of other noises

Comprehensively considering the possible noises, possible noises other than the above noises are as follows: (1) spurious electronic phase-shifts, which result from the temperature or stress fluctuations of the cables and the phasemeter's analog front-end circuit. Previous work showed that it mainly affected the path-length measurement sensitivity in the frequency range of 0.1–10 mHz [21, 42]; (2) parasitic signals noise, which is caused by ghost beams, electrical cross coupling and so on; (3) photo-detector electronic noise, the low SNR of which affects the measuring accuracy of the phase measurement system [42]. However, limited by the great background noise of the laser interferometer, how the above noises affect the ranging accuracy cannot be quantitatively evaluated under the current condition, but the related experiments and simulations will be carried out.

3.7 Performance of characterizing the motion of the simulated testmass

To better understand the measurement sensitivity of the laser interferometer prototype, a dynamic measuring mode was adopted to evaluate the performance of characterizing the motion of the simulated testmass, of which the measurement principle is as follows: the simulated testmass (here replaced by a mirror) located on the left side of the optical bench is installed on a nano-positioning stage (Physik Instrumente, P-772K012), which moves in the form of a sine wave (peak to peak amplitude $A = 100$ pm, period $T = 10$ s), and keeps the environmental condition as stable as possible, and the measuring data are analyzed with amplitude spectrum (AS).

The path-length measurement sensitivity obtained from the laser interferometer is presented in Fig. 9, from which it can be derived that the path-length measurement sensitivities of the two measurement interferometers are better
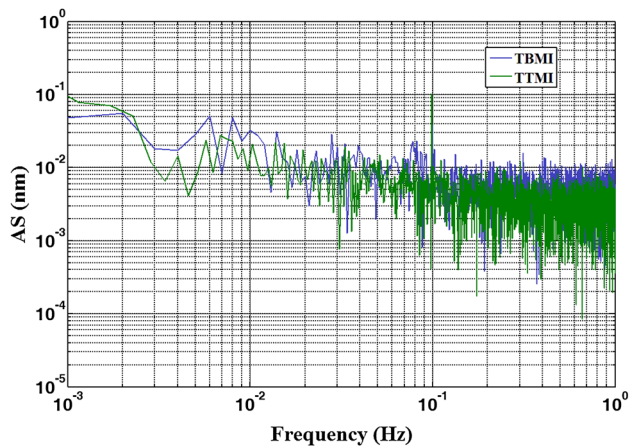
Fig. 9 Performance of characterizing the motion of the simulated testmass

than 100 pm in the frequency band of 1 mHz–1 Hz. Within the higher frequency range of 0.01–1 Hz, the sensitivity is better than 30 pm, but in the lower frequency range of 1–10 mHz, the noise level increases with decreasing frequency mainly because of the thermal noise resulting from the temperature fluctuations. The two peaks corresponding to 0.1 Hz resulting from the modulated signal show that this laser interferometer prototype can characterize the motion of the simulated testmass quite well. So laboratory activities have demonstrated the feasibility of this heterodyne interferometer of measuring the tiny fluctuations of the testmass caused by the simulated gravitational waves or gravity fields.

4 Conclusions and outlook

Some results of investigations on an on-ground polarizing laser interferometer prototype used for path-length fluctuations measurement were presented. The results show that the path-length measurement sensitivity of the laboratory prototype is better than 200 pm/Hz$^{1/2}$ in the frequency band of 10 mHz–1 Hz, and the performance of characterizing the motion of the simulated testmass is better than 100 pm inside the frequency range of 1 mHz–1 Hz. But all the results are just the beginning of efforts in China toward mapping the Earth's gravity fields and detecting gravitational waves. There are still many key techniques to be solved, such as laser pointing modulation, laser arm-locking, laser phase-locking control, time delay interferometry and relative time and frequency alignment. Next step, using hydroxy-catalysis or other surface bonding techniques to fix the optics on an ultra-stable glass-ceramic baseplate made of Clearceram or Zerodur and lowering the pressure of the vacuum chamber to further

reduce the thermal noise is being planned, and implementing laser pointing and laser phase-locking control into this prototype is being considered. Besides, adopting another nano-positioning stage to drive the mirror located on the right side of the optical bench to simulate a displacement caused by the orbit drift, and using the existing nano-positioning stage on the left side to simulate the science signals resulting from gravitational waves or gravity variations of the planet are the primary task in our future work, in considering how to identify and extract the science signal from the Doppler shift between the two spacecraft.

References

1. K. Danzmann, The LISA study team, Class. Quantum Gravity **13**, A247 (1996)
2. K. Danzmann for the LISA Study Team, Class. Quantum Gravity **14**, 1399 (1997)
3. K. Danzmann for the LISA Study Team, Adv. Space Res. **25**, 1129 (2000)
4. R. Reinhard, ESA Bull. **103**, 36 (2000)
5. N. Seto, S. Kawamura, T. Nakamura, Phys. Rev. Lett. **87**, 221103 (2001)
6. A. Hammesfahr, Class. Quantum Gravity **18**, 4045 (2001)
7. T. Edwards, M.C.W. Sandford, Acta Astronaut. **48**, 549 (2001)
8. O. Jennrich, Nucl. Phys. B **113**, 282 (2002)
9. K. Danzmann, A. Rüdiger, Class. Quantum Gravity **20**, S1 (2003)
10. P.L. Bender, Class. Quantum Gravity **21**, S1203 (2004)
11. V. Corbin, N.J. Cornish, Class. Quantum Gravity **23**, 2435 (2006)
12. G.M. Harry, P. Fritschel, D.A. Shaddock, W. Folkner, E.S. Phinney, Class. Quantum Gravity **23**, 4887 (2006)
13. P.L. Bender, M.C. Begelman, J.R. Gair, Class. Quantum Gravity **30**, 165017 (2013)
14. G. Heinzel, C. Braxmaier, K. Danzmann, P. Gath, J. Hough, O. Jennrich, U. Johann, A. Rüdiger, M. Sallusti, H. Schulte, Class. Quantum Gravity **23**, S119 (2006)
15. O. Jennrich, P. Binetruy, M. Colpi, K. Danzmann, P. Jetzer, A. Lobo et al., Assessment study report, ESA/SRE **19** (2012)
16. S. Nagano, M. Hosokawa, H. Kunimori, T. Yoshino, S. Kawamura, M. Ohkawa, T. Sato, Rev. Sci. Instrum. **76**, 124501 (2005)
17. R. Rummel, in *Towards an Integrated Global Geodetic Observing System (IGGOS), Munich, Germany, 5–9 October (1998)*, Vol. 12 (Springer, 2000)
18. S. Nagano, T. Yoshino, H. Kunimori, M. Hosokawa, S. Kawamura, T. Sato, M. Ohkawa, Meas. Sci. Technol. **15**, 2406 (2004)
19. M. Dehne, F.G. Cervantes, B. Sheard, G. Heinzel, K. Danzmann, J. Phys: Conf. Ser. **154**, 012023 (2009)
20. R.T. Stebbins, Class. Quantum Gravity **26**, 094014 (2009)
21. B.S. Sheard, G. Heinzel, K. Danzmann, D.A. Shaddock, W.M. Klipstein, W.M. Folkner, J. Geod. **86**, 1083 (2012)
22. P.L. Bender, R. Nerem, J. Wahr, Space Sci. Rev. **108**, 385 (2003)

23. M. Horwath, J.M. Lemoine, R. Biancale, S. Bourgogne, J. Geod. **85**, 23 (2011)
24. R. Pierce, J. Leitch, M. Stephens, P. Bender, R. Nerem, Appl. Opt. **47**, 5007 (2008)
25. J. Lhermite, A. Desfarges-Berthelemot, V. Kermene, A. Barthelemy, Opt. Lett. **32**, 1842 (2007)
26. X.F. Gong, S.N. Xu, S. Bai, Z.J. Cao, G.R. Chen, Y.B. Chen, X.K. He, G. Heinzel, Y.K. Lau, C.Z. Liu, J. Luo, Z.R. Luo et al., Class. Quantum Gravity **28**, 094012 (2011)
27. S.F.P. Zwart, E.P.K. van den Heuvel, Nature **450**, 388 (2007)
28. M.C. Miller, D.P. Hamilton, Mon. Not. R. Astron. Soc. **330**, 232 (2002)
29. M.C. Miller, Astrophys. J. **581**, 438 (2002)
30. M.C. Miller, E.J.M. Colbert, Int. J. Mod. Phys. D **13**, 1 (2004)
31. M.A. Gürkan, J.M. Fregeau, F.A. Rasio, Astrophys. J. **640**, L39 (2006)
32. A. Heger, S.E. Woosley, Astrophys. J. **567**, 532 (2002)
33. P. Madau, M.J. Rees, Astrophys. J. **551**, L27 (2001)
34. Y.Q. Li, Z.R. Luo, H.S. Liu, Y.H. Dong, G. Jin, Chin. Phys. Lett. **29**, 079501 (2012)
35. H.C. Yeh, Q.Z. Yan, Y.R. Liang, Y.W. Wang, J. Luo, Rev. Sci. Instrum. **82**, 044501 (2011)
36. P. Amaro-Seoane, G. Auger, S. Babak et al., *eLISA Whitepaper-RC1* (eLISA Working Group, 2013), pp. 13, 14
37. F. Antonucci, M. Armano, H. Audley et al., Class. Quant. Grav. **28**, 094002 (2011)
38. S.J. Mitryk, G. Mueller, J. Sanjuan, Phys. Rev. D **86**, 12006 (2012)
39. G. Heinzel, C. Braxmaier, M. Caldwell, K. Danzmann, F. Draaisma, A. García, J. Hough, O. Jennrich et al., Class. Quantum Gravity **22**, S149 (2005)
40. M. Armano, M. Benedetti, J. Bogenstahl, D. Bortoluzzi, P. Bosetti, N. Brandt, A. Cavalleri, G. Ciani et al., Class. Quantum Gravity **26**, 094001 (2009)
41. M. Dehne, M. Trobs, G. Heinzel, K. Danzmann, Opt. Express **20**, 27273 (2012)
42. H.S. Liu, Y.H. Dong, Y.Q. Li, Z.R. Luo, G. Jin, Rev. Sci. Instrum. **85**, 024503 (2014)
43. T. Westphal, G. Bergmann, A. Bertolini, M. Born, Y. Chen, A.V. Cumming et al., Appl. Phys. B **106**, 551 (2012)